Catalysis Today 183 (2012) 124–129

Contents lists available at SciVerse ScienceDirect

Catalysis Today

journal homepage: www.elsevier.com/locate/cattod

Moving from surfactant-stabilized aqueous rhodium (0) colloidal suspension to heterogeneous magnetite-supported rhodium nanocatalysts: Synthesis, characterization and catalytic performance in hydrogenation reactions

Carl-Hugo Pélisson[a,b], Lucas L.R. Vono[c], Claudie Hubert[a,b], Audrey Denicourt-Nowicki[a,b], Liane M. Rossi[c], Alain Roucoux[a,b,*]

[a] Ecole Nationale Supérieure de Chimie de Rennes, CNRS, UMR 6226, Avenue du Général Leclerc, CS 50837, 35 708 Rennes Cedex 7, France
[b] Université Européenne de Bretagne, France
[c] Instituto de Química, Universidade de São Paulo, Av. Prof. Lineu Prestes 748, São Paulo 05508-000, SP, Brazil

ARTICLE INFO

Article history:
Received 6 July 2011
Received in revised form 31 August 2011
Accepted 31 August 2011
Available online 5 October 2011

Keywords:
Metallic nanoparticles
Magnetic support
Impregnation
Hydrogenation
Recycling

ABSTRACT

Wet impregnation of pre-synthesized surfactant-stabilized aqueous rhodium (0) colloidal suspension on silica was employed in order to prepare supported Rh^0 nanoparticles of well-defined composition, morphology and size. A magnetic core–shell support of silica (Fe_3O_4@SiO_2) was used to increase the handling properties of the obtained nanoheterogeneous catalyst. The nanocomposite catalyst Fe_3O_4@SiO_2-Rh^0 NPs was highly active in the solventless hydrogenation of model olefins and aromatic substrates under mild conditions with turnover frequencies up to 143,000 h^{-1}. The catalyst was characterized by various transmission electron microscopy techniques showing well-dispersed rhodium nanoparticles (~3 nm) mainly located at the periphery of the silica coating. The heterogeneous magnetite-supported nanocatalyst was investigated in the hydrogenation of cyclohexene and compared to the previous surfactant-stabilized aqueous Rh^0 colloidal suspension and various silica-supported Rh^0 nanoparticles. Finally, the composite catalyst could be reused in several runs after magnetic separation.

1. Introduction

A great but still largely unmet goal of modern catalysis is to transfer to heterogeneous catalysis the synthetic control of nanoparticle synthesis in solution by the bottom-up approach. Despite recent exciting progress in nanocatalysis [1,2], the preparation of supported nanoparticles with precise control over factors such as composition, size, size-distribution and shape remains a challenge. In that context, can we bring what has been learned in the modern "soluble nanoparticle catalysts" [3–5] to the development of supported-nanoparticle heterogeneous catalysts [6], which will be more suitable for industrial applications [7–9].

In general, supported nanoparticles on solids such as oxides, carbon or zeolites are prepared by various deposition–precipitation or co-precipitation procedures, oxidation–reduction steps and the nanoparticle size is tentatively adjusted by varying experimental parameters such as the pH, the reducing agent, the concentration of precursors in solution and the temperature of calcinations [10]. Another very elegant strategy consists of the immobilization of pre-synthesized metal nanoparticles [11]. In that case, the control on particles size and shape obtained in solution will be better than any method to prepare supported metal particles by reduction and/or deposition of metal precursors over solid supports.

Among other attempts to improve the reusability of "soluble metal nanocatalysts", the development of biphasic catalytic conditions, such as biphasic aqueous/organic systems [12,13] or ionic-liquid/organic systems [14,15] have largely been developed. In those systems, the catalysts are stabilized in the aqueous or ionic liquid phase and the product/organic phase can be collected by phase decantation. The catalyst-containing phase is easily recovered and recycled, although the catalytic rates are compromised because of mass-transfer limitations. Metal nanoparticles deposited on solid supports, which typically increase the reaction rates by few orders of magnitude, have emerged as sustainable alternatives to conventional materials [1]. Magnetically driven separation of catalysts immobilized on magnetic supports by just applying an external magnetic field to the reaction mixture has recently received great attention as a non-laborious, cheap and often highly scalable technique [16,17] although the early research in the field of magnetic nanoparticles can be dated back several decades. A variety of methodologies have been reported in the literature for the immobilization of homogeneous and

* Corresponding author at: Ecole Nationale Supérieure de Chimie de Rennes, CNRS, UMR 6226, Avenue du Général Leclerc, CS 50837, 35 708 Rennes Cedex 7, France. Fax: +33 223 23 80 37.
E-mail address: alain.roucoux@ensc-rennes.fr (A. Roucoux).

0920-5861/$ – see front matter © 2011 Elsevier B.V. All rights reserved.
doi:10.1016/j.cattod.2011.08.046

heterogeneous catalysts on such kind of supports possessing superparamagnetic properties. The developed approaches include the direct deposition of metals on magnetic nanoparticles, the functionalization of magnetic particle surfaces or the coating of the magnetic cores with inorganic or organic materials before metal loading. The use of inorganic oxides, such as SiO_2, is a strategy to give an extra protection to naked iron oxides (especially magnetite) against oxidation and to help the immobilization of catalysts through a covalent approach [18–23]. This methodology was efficiently used to prepare Fe_3O_4@SiO_2-NH_2-Rh^0 NPs and relies on the uptake of Rh^{3+} by amino-functionalized silica-coated magnetic nanoparticles followed by metal reduction under controlled H_2 conditions [24]. Tremendous efforts are still ongoing to improve the preparation of supported metal NP catalysts with good control of composition, morphology, and size distribution. The examples of magnetically recoverable metal NP catalysts found in the literature are based on reduction of metal precursors over a magnetic solid.

Recently, we have described a simple methodology based on the wet impregnation onto an inorganic matrix of a pre-stabilized aqueous colloidal rhodium suspension. SiO_2-Rh^0 NPs [25,26] and TiO_2-Rh^0 NPs [27,28] were prepared by this method and well characterized in terms of organization and size. In this paper, we described the immobilization of Rh^0 NPs on the silica coated magnetite core–shell support. Fe_3O_4@SiO_2-Rh^0 NPs material was prepared by impregnation of the inorganic silica coating of the magnetite core by pre-synthesized aqueous Rh^0_{coll} suspension. The composite catalyst was characterized by transmission electron microscopy (TEM, HTREM) and evaluated in the hydrogenation of cyclohexene at 75 °C and 6 bar of H_2 in comparison with SiO_2-Rh^0 NPs, the aqueous Rh^0_{coll} suspension and the analogous Fe_3O_4@SiO_2-NH_2-Rh^0 NPs. Finally, the heterogeneous magnetite-supported rhodium nanocatalyst was investigated in the solventless hydrogenation of model olefins and aromatic substrates under mild conditions as well as its stability and reusability.

2. Experimental

2.1. General

Rhodium trichloride was obtained from Strem Products. Sodium borohydride, all the organic compounds investigated as substrates were purchased from Acros Organics or Sigma–Aldrich–Fluka and used without further purification. Water was distilled twice before use by conventional method. The *N*,*N*-dimethyl-*N*-cetyl-*N*-(2-hydroxyethyl) ammonium chloride and tetrafluoroborate salts (HEA16X, X = Cl or BF_4) were synthesised as previously described [29] and the *N*-cetyl-*N*-tris-(2-hydroxyethyl) ammonium chloride (THEA16Cl) was prepared by quaternarization of hexadecylamine with chloroethanol [30]. The silica was obtained from Merck and presents the following characteristics: mean diameter: 80 μm, pore diameter 5.4 nm, specific area 490 $m^2\,g^{-1}$, pore volume 0.77 $cm^3\,g^{-1}$ and internal porosity 58%.

2.2. Synthesis of magnetic particles supported Rh^0 nanoparticles

2.2.1. Synthesis of the silica-coated magnetic nanoparticles

The silica-coated magnetic particles were prepared by a reverse microemulsion method reported elsewhere [24]. To 44.6 g of polyoxyethylene (5) isooctylphenyl ether surfactant dispersed in 600 mL of cyclohexane was added oleic acid coated magnetite (200 mg). After the addition of 9.44 mL NH_4OH (29% aqueous solution), the microemulsion was formed and 7.7 mL of TEOS were added. The reaction mixture was slowly stirred during 16 h. Then, 200 mL of methanol was added and the alcoholic phase was centrifuged (7000 rpm, 10 min). After washing with ethanol and centrifugation, the silica-coated magnetic particles were dried under vacuum.

2.2.2. Preparation of the surfactant-stabilized aqueous Rh^0 colloidal suspension

To an aqueous solution of the ammonium surfactant HEA16X (with X = Cl or BF_4) or THEA16Cl (2 eq., 7.6×10^{-4} mol, 95 mL H_2O), was added 36 mg of sodium borohydride (9.5×10^{-4} mol, 2.5 eq.). Then this solution was quickly added under vigorous stirring to an aqueous solution (5 mL) of the precursor $RhCl_3{\cdot}3H_2O$ (100 mg, 3.8×10^{-4} mol) to obtain a stable aqueous Rh^0 colloidal suspension (100 mL). The reduction occurs instantaneously and is observed by a colour change from red to black. The Rh^0_{coll} suspension was stirred overnight before use.

2.2.3. Metal immobilization on silica-coated magnetic particles

This preparation follows the preparation of SiO_2-supported metallic nanoparticles reported elsewhere [26]. The magnetic support (50 mg) was dispersed in distilled water (2.5 mL). After addition of the ammonium surfactant (2 eq.), the mixture was stirred at room temperature overnight. The adequate amount of the pre-stabilized Rh^0 nanoparticles (0.1 wt%) was added and the mixture was stirred for 2 h. The particles were magnetically separated and dried at 100 °C.

2.3. General procedure for the solventless hydrogenation of the cyclohexene under 6 bar of H_2

Catalytic reactions were carried out in a modified Fischer–Porter glass reactor connected to a pressurized dihydrogen gas supply tank. The Fischer–Porter bottle was set at a constant pressure for the entire course of the reaction by leaving the reactor connected to the dihydrogen gas supply through a gas regulator set to the desired pressure. In a typical experiment, the catalyst (35 mg of magnetic solid, 3×10^{-4} mmol Rh), cyclohexene (1.2 g, 14.6 mmol) and a magnetic stir bar were added to the reactor under inert atmosphere. The reactor was evacuated and connected to the dihydrogen gas supply apparatus for gas admission. The reaction was conducted under magnetic stirring (700 rpm) at 6 bar and 75 °C. The temperature was maintained constant by a hot-stirring plate connected to a digital temperature controller. The reactions were monitored by the fall in the pressure of the dihydrogen gas supply tank until completion. After the dihydrogen gas consumption stopped, the catalyst was recovered magnetically by placing a magnet on the reactor wall and the products were collected and analyzed by gas chromatography (GC).

2.4. General procedure for the solventless hydrogenation of model olefins and aromatic substrates under 10 bar of H_2

Catalytic reactions were carried out in a stainless steel autoclave under magnetic stirring. In a typical experiment, the reactor was charged with the catalyst Fe_3O_4@SiO_2-Rh^0 NPs (37.6 mg, 3.6×10^{-4} mmol of Rh^0) and a magnetic stir bar. Then, the appropriate substrate (14.6 mmol) was added to the autoclave and the dihydrogen was admitted to the system at the desired pressure (10 bar). The system was purged with H_2 three times after that the reaction was magnetically stirred until completion. The complete conversion was followed by GC analysis.

2.5. Transmission electron microscopy

Samples for TEM observations were prepared by placing a drop containing the nanoparticles in carbon coated TEM grids. The transmission electron microscopy (TEM) work was partially performed at the C2NANO – Center for Nanoscience and Nanotechnology

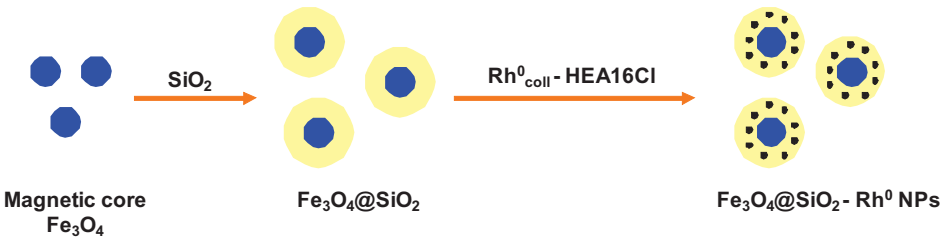

Fig. 1. Preparation of Fe_3O_4@SiO_2-Rh^0 NPs.

(LNLS, Campinas, SP, Brazil) using a JEOL-3010 ARP microscope and at the Institut des Matériaux de Paris-Centre – Université Pierre et Marie Curie using a JEOL JEM 2010 UHR microscope.

3. Results and discussion

We here describe the immobilization of pre-synthesized surfactant-stabilized aqueous Rh^0 colloidal NPs on a silica coated magnetite core–shell support, as depicted in Fig. 1. The aqueous Rh^0 colloidal (Rh^0_{coll}) suspension was prepared by chemical reduction of an aqueous solution of rhodium chloride salt in the presence of water-soluble ammonium salts as stabilizing agents and fully characterized as previously reported elsewhere [29,30]. The core–shell magnetic support comprised of magnetite nanoparticles spherically coated with silica (Fe_3O_4@SiO_2) was synthesized and characterized as also previously reported by some of us [24]. Based on the method we have previously developed for the deposition of metallic nanospecies on an inorganic support such as SiO_2 or TiO_2 [26,28], the wet impregnation of the silica coated magnetic particles Fe_3O_4@SiO_2 was investigated at room temperature using pre-synthesized aqueous Rh^0_{coll} suspensions. Various protective agents (HEA16Cl, Br or THEA16Cl salts) were tested both to stabilize the Rh^0 NPs and to facilitate the impregnation process. The results are gathered in Table 1 and the metal loading was checked by ICP AES analysis and compared to the nominal value.

First, concerning the choice of the surfactant, the metal loading is much better using HEA16Cl or HEA16BF_4 as surfactants (Table 1, entries 1 and 3) and very close to the nominal value (0.1 wt%), compared to THEA16Cl (Table 1, entry 4). After several experiments we have seen that metal loadings up to 0.5 wt% could also be obtained with the same Rh^0_{coll}-HEA16Cl suspension containing a molar ratio Rh/HEA16Cl = 2 (Table 1, entry 2). However, attempts to get higher metal loadings close to 1 wt% were unfruitful.

In a first approach, we have compared the catalytic performance of the optimized system with previously described Rh^0 NP catalysts in the hydrogenation of cyclohexene at 75 °C and 6 bar H_2 (Table 2). The turnover frequencies (TOFs) were calculated considering an optimized reaction time for complete conversion of the substrate and based on the introduced amount of metal and not on the exposed surface metal and thus may be underestimated. As previously reported by Janiak et al. [31], the catalytic activity results not only from the exposed surface metal atoms since the surface can restructure, atoms can shift positions during heterogeneous processes and partial aggregation could occur during catalysis, modifying the fraction of surface atoms. These changes in the surface render the determination of the number of surface atoms difficult.

The Fe_3O_4@SiO_2-Rh^0 NP catalyst with 0.09 wt% Rh loading determined by ICP AES (0.1 wt% nominal value, Table 1, entry 1) was evaluated with a turnover number of 43,000 mol of substrate per mol of metal (total metal) and showed very high catalytic activities up to 143,000 h^{-1} with total conversion of the substrate after 0.3 h (Table 2, entry 1). As a reference, the use of the colloidal suspension Rh^0_{coll}-HEA16Cl leads to the conversion of cyclohexene into cyclohexane with a TOF of 33,000 h^{-1} in the same catalytic conditions (Table 2, entry 3). Consequently, the TOF observed with the heterogeneous magnetite-supported rhodium nanocatalysts is 4.3 times the catalytic activity of Rh^0_{coll}-HEA16Cl used under biphasic conditions (Table 2, entries 1 and 3). Moreover, the performance of the Fe_3O_4@SiO_2-Rh^0 NPs was also superior to the Rh^0 NPs prepared by impregnation of Rh^{3+} ions followed by *in situ* H_2 reduction over the same magnetic solid (Fe_3O_4@SiO_2 with 0.1 wt% of Rh) and thus showed the advantage of the use of pre-formed nanoparticles (Table 2, entries 1 and 4). In that case, the turnover frequency is enhanced by a factor of 70 when using pre-synthesized Rh^0 NPs. The reduction of Rh^{3+} ions by $NaBH_4$ leads to a significant increase in catalytic activity (Table 2, entry 6). This result could be explained by a better reduction of the metal salts using this strong reductive agent, providing zerovalent rhodium nanoparticles with a suitable size for catalytic applications. Indeed, the same catalyst prepared by *in situ* H_2 reduction with 1.5 wt% Rh loading decreases the catalytic reaction time from 21 h to 3 h in the same conditions probably due to a better growth processes giving a suitable nanoparticle size for catalytic applications (Table 2, entry 5). Finally, a weak influence of the silica support was also observed when comparing the immobilization process on commercially available silica instead of

Table 1
Optimization of the synthesis of Fe_3O_4@SiO_2-Rh^0 NPs: choice of the surfactant.

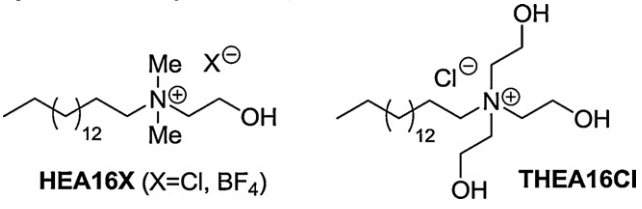

Entry	Surfactant	Equivalents of surfactant	$Rh_{theorical}$ (wt%)	$Rh_{E.A.}$ (wt%)[a]
1	HEA16Cl	2	0.1	0.09
2	HEA16Cl	2	0.5	0.5
3	HEA16BF_4	2	0.1	0.09
4	THEA16Cl	2	0.1	0.02

[a] Determined by atomic absorption analysis (ICP AES).

Table 2
Comparison of various catalysts in the hydrogenation of cyclohexene at 75 °C and 6 bar H_2.

Entry	Catalyst	Rh loading (%)	TON[g]	Time (h)	TOF (h^{-1})[h]
1	Fe_3O_4@SiO_2-Rh^0 NPs[a]	0.09[e]	43,000	0.3	143,000
2	SiO_2-Rh^0 NPs[b]	0.08[e]	35,600	0.3	120,000
3	Rh^0_{coll}-HEA16Cl[a]	–	43,000	1.3	33,000
4	Fe_3O_4@SiO_2-NH_2-Rh^0 NPs[c]	0.1[f]	43,000	21	2,000
5	Fe_3O_4@SiO_2-NH_2-Rh^0 NPs[c]	1.5[f]	35,600	3	12,000
6	Fe_3O_4@SiO_2-NH_2-Rh^0 NPs[d]	0.1[f]	35,600	0.57	62,500

[a] This work.
[b] Catalyst prepared according to Ref. [26].
[c] Supported Rh^0 NPs prepared by impregnation of Rh^{3+} ions followed by *in situ* H_2 reduction prepared according to Ref. [24].
[d] Supported Rh^0 NPs obtained by the reduction of Rh^{3+} ions with $NaBH_4$.
[e] Determined by ICP AES in this set of experiments.
[f] Nominal value.
[g] TON = mol substrate converted per mol catalyst (total metal).
[h] TOF = mol substrate converted per mol catalyst (total metal) per hour at 100% conversion.

the silica coated magnetite core–shell support (Table 2, entries 1 and 2). In fact, the catalytic activity of the SiO_2-Rh^0 NPs with a TOF of 120,000 h^{-1} was very close to the value observed for Fe_3O_4@SiO_2-Rh^0 NPs. This result could be explained by heterogeneous surface properties of silica. In fact, different preparation method and post-treatments have been used providing different characteristics of silica based supports in terms of surface area, pore and grain sizes.

In a second step, the Fe_3O_4@SiO_2-Rh^0 NPs stability and reusability were studied in the solventless hydrogenation of cyclohexene with turnover number as high as 40,000 mol of substrate per mol of metal (total metal) at 75 °C and 6 bar H_2. The catalyst was easily recovered by placing a magnet in the reactor wall and reused for several runs with >99% conversion. The catalytic activity remains constant on the first three runs (accumulated TON of 129,000 mol/mol) with TOF values ~143,000 h^{-1}. However, a slight decrease in the catalytic activity was observed starting the fourth run, although the catalyst remains active for up to 7 cycles with accumulated TON of 300,000 mol/mol. The atomic absorption analysis (ICP AES) of the recovered catalyst confirmed the presence of 93% of the initial metal loading after 7th run (0.084 in the spent catalyst *vs.* 0.09 wt%). Consequently, the decrease in kinetic properties of the catalyst is not only explained by metal leaching but also by other deactivation processes such as particles aggregation or poisoning effect.

In a third set of experiments, we investigated the hydrogenation of several olefins and various benzene derivatives with a turnover number of 40,000 mol of substrate per mol of metal (total metal) under standard conditions (10 bar H_2, room temperature). These experimental conditions have been used to activate the reaction and limit the time in the case of less reducible substrates as aromatic compounds. Indeed, no reduction was observed under atmospheric hydrogen pressure in opposition with the use of the aqueous suspension of Rh^0_{coll}-HEA16Cl in biphasic conditions [13]. The conversion was followed by GC analysis or

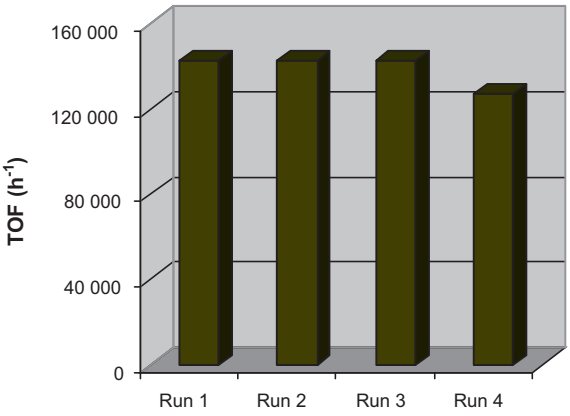

Fig. 2. Cyclohexene hydrogenation at 75 °C and 6 bar H_2: recycling experiments with Fe_3O_4@SiO_2-Rh^0 NPs (TON each run = 43,000).

determined for a defined time (6 h). The results are gathered in Table 3.

As model olefinic substrates, cyclooctene and tetradecene (Table 3, entries 1 and 2) have been investigated. An efficient turnover frequency was observed in the hydrogenation of the lipophilic tetradecene (TOF = 32,000 h^{-1}) but a significant decrease was obtained with the cyclic compound. This result could be explained by the rigid ring leading to a more steric hindrance around the particle and thus limiting the accessibility of the reducible C–C double bond to the active sites. We have also studied the hydrogenation of substituted aromatic compounds. The best activities were observed for toluene hydrogenation with a complete conversion in 2.5 h providing a TOF = 16,000 h^{-1} (Table 3, entry 5). In the same time, styrene was transformed in a mixture of ethylbenzene and ethylcyclohexane (ratio 70/30, Table 3, entry 3). After 4 h, 70% of ethylcyclohexane was obtained (Table 3, entry

Table 3
Catalytic investigation of olefins and aromatic derivatives with Fe_3O_4@SiO_2-Rh^0 NPs.[a]

Entry	Substrate	Product (%)	Time (h)	TOF (h^{-1})[b]
1	Cyclooctene	Cyclooctane (100)	2.5	16,000
2	Tetradecene	Tetradecane (100)	1.25	32,000
3	Styrene	Ethylbenzene/Ethylcyclohexane (70/30)	2	20,000
4	Styrene	Ethylbenzene/Ethylcyclohexane (30/70)	4	10,000
5	Toluene	Methylcyclohexane (100)	2.5	16,000
6	*p*-Xylene	*p*-dimethylcyclohexane (cis/trans:75/25)	6	6,667
7	*iPr*-Benzene	*iPr*-cyclohexane (15)	6	n.c.[c]
8	Anisole	Methoxycyclohexane (10)	6	n.c.[c]
9	*m*-Cresol	*m*-Methylcyclohexanol (1.5)	6	n.c.[c]

[a] Fe_3O_4@SiO_2-Rh^0 NPs (37.6 mg, 3.6×10^{-4} mmol of Rh^0), substrate (14.6 mmol), 10 bar H_2, room temperature.
[b] TOF = mol substrate converted per mol catalyst (total metal) per hour at 100% conversion.
[c] Not calculated.

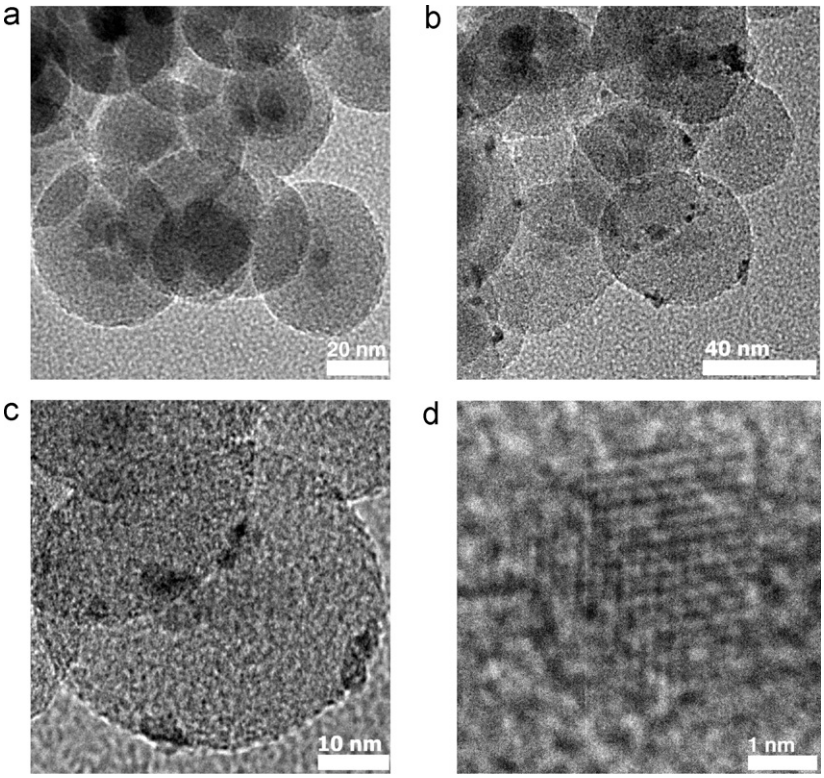

Fig. 3. TEM images of (a) Fe_3O_4@SiO_2 catalyst support, (b) Fe_3O_4@SiO_2-Rh^0 NPs catalyst, (c) detail of Fe_3O_4@SiO_2-Rh^0 NPs catalyst showing Rh^0 at the surface of the silica and (d) high resolution (HRTEM) of a single Rh^0 NP over the support with an average diameter of about 3 nm (scale bar = 1 nm).

4), showing no deactivation of the catalyst during the process and a complete conversion could be observed after a more important reaction time. When we compared alkylated derivatives such as toluene, *p*-xylene and *iPr*-benzene, the presence of bulkier substituents on the aromatic ring tends to decrease the kinetic properties. Indeed, a total conversion was obtained in a double time (6 h) for the hydrogenation of *p*-xylene as a model disubstituted compound (TOF = 6667 h^{-1}, Table 3, entry 6) in opposition with the toluene as a monoalkyl-substituted derivative (TOF = 16,000 h^{-1}, Table 3, entry 5). Similarly, a lower activity was also observed with *iPr*-benzene (Table 3, entry 7). This phenomenon has already been reported in various media [32] and could be explained by an increased steric hindrance on the aromatic ring that limits the access to the Rh^0 species on the silica coated magnetite core–shell support. Finally, the hydrogenation of functionalized oxygenated aromatic substrates such as anisole or cresol derivatives, which correspond to model lignin compounds, was also investigated. These reactions could be an advanced step for the production of fuels from biomass [33]. Unfortunately, very poor results were obtained, proving the difficulties to reduce functionalized aromatic derivatives with Fe_3O_4@SiO_2-Rh^0 NPs in mild conditions in terms of hydrogen pressure and short reaction time Fig. 2.

The morphology and the location of the Fe_3O_4@SiO_2-Rh^0 NPs catalyst were assessed from analysis of transmission electron microscopy (TEM) micrographs such as presented in Fig. 3. The support is comprised of magnetic cores (Fe_3O_4 ~ 8–10 nm) well-coated with silica (Fig. 3a). The rhodium nanoparticles (~3 nm) are mainly located at the periphery of the silica coating with good dispersion (Fig. 3b and c). High resolution TEM was also carried out (Fig. 3d). Analyses of the fast Fourier transformation (FFT) of the HRTEM images reveal the presence of inter-reticular distances of nearly 0.2196 nm and 0.1902 nm, which are characteristic of the (1 1 1) and (2 0 0) lattice planes of Rh^0 and different from the Fe nanoparticles (2.53 and 2.96 nm).

4. Conclusion

We have described a synthetic methodology based on the use of pre-synthesized metal nanoparticles to develop supported Rh^0 NPs over silica-based supports. This approach takes advantage of the recent advances in the synthesis of size, shape and composition-controlled metal and magnetic oxide nanomaterials, which were efficiently combined to formulate pertinent nanocomposite catalysts. An important feature is that the developed strategy allows metal nanoparticles to be well-dispersed on support surfaces, selection of the desired support properties, as for example, the magnetic support used in this study, and by choosing the metal nanoparticles synthesis one can select the desired particle size and shape with few restrictions on their surface properties. The magnetically recoverable Rh^0 nanocatalyst prepared by using surfactant-stabilized Rh^0 NPs proved to be highly active in the hydrogenation of cyclohexene (TOF = 143,000 h^{-1}) and usual benzene derivatives with TOF up to 20,000 h^{-1}. The overall performance of the supported NPs is improved if compared to its activity as a soluble NP catalyst and the magnetic properties allow the catalyst to be isolated and recycled by the assistance of an external magnet, which greatly simplifies the work-up procedure and purification of products minimizing the use of solvents, costly consumables, energy and time. Also, the pre-formed Rh^0 NPs are prepared through reproducible and well-controlled syntheses in opposition to traditional colloids, which is a major advantage of this methodology.

Acknowledgements

The authors are grateful to the Région Bretagne (PhD fellowships – MAGFOCAT and PARTICAT programs) for financial supports and the Université Européenne de Bretagne for the international mobility grant to C. Hubert. They also thank the support from

the international cooperation programs PICS Brazil-France (grant nos. 490678/2008-4 and 3637/2007-2010) and CAPES-COFECUB (grant nos. 965/09 and Ph695/10). Support from the Brazilian agencies CNPq and FAPESP is also acknowledged. The authors are indebted to Patricia Beaunier from Université Pierre et Marie Curie, and C2NANO – Center for Nanoscience and Nanotechnology/MCT (Brazil) for TEM images.

References

[1] V. Polshettiwar, R.S. Varma, Green Chem. 112 (2010) 743–754.
[2] N. Yan, C.X. Xiao, Y. Kou, Coord. Chem. Rev. 254 (2010) 1179–1218.
[3] D. Astruc, F. Lu, J.R. Aranzaes, Angew. Chem. Int. Ed. 44 (2005) 7852–7872.
[4] J.A. Widegren, R.G. Finke, J. Mol. Catal. A: Chem. 198 (2003) 317–341.
[5] A. Roucoux, J. Schulz, H. Patin, Chem. Rev. 102 (2002) 3757–3778.
[6] K. Mori, H. Yamashita, Phys. Chem. Chem. Phys. 12 (2010) 14420–14432.
[7] J. Grunes, J. Zhu, A. Somorjai, Chem. Commun. (2003) 2257–2260.
[8] V. Ponec, G.C. Bond, Catalysis by metals and alloys, in: B. Delmon, Y.T. Yates (Eds.), Studies in Surface Science and Catalysis, Elsevier, Amsterdam, 2005.
[9] G. Ertl, H. Knoezinger, J. Weitkamp, Catalytic Process. Part B. Handbook of Heterogeneous Catalysis, Wiley-VCH, New-York, 1997.
[10] J.M. Campelo, D. Luna, R. Luque, J.M. Marinas, A.A. Romero, ChemSusChem 2 (2009) 18–45.
[11] N. Zheng, G.D. Stucky, J. Am. Chem. Soc. 128 (2006) 14278–14280.
[12] B. Cornils, Org. Process Res. Dev. 2 (1998) 121–127.
[13] J. Schulz, S. Levigne, A. Roucoux, H. Patin, Adv. Synth. Catal. 344 (2002) 266–269.
[14] J. Dupont, D. de Oliveira Silva, Transition-metal nanoparticle catalysis in imidazolium ionic liquids, in: D. Astruc (Ed.), Nanoparticles and Catalysis, Wiley-VCH, Weinheim, 2008, pp. 195–218.
[15] J. Dupont, G.S. Fonseca, A.P. Umpierre, P.F.P. Fichtner, S.R. Teixeira, J. Am. Chem. Soc. 124 (2002) 4228–4229.
[16] V. Polshettiwar, R. Luque, A. Fihri, H.B. Zhu, M. Bouhrara, J.M. Bassett, Chem. Rev. 111 (2011) 3036–3075.
[17] S. Shylesh, V. Schunemann, W.R. Thiel, Angew. Chem. Int. Ed. 49 (2010) 3428–3459.
[18] L.M. Rossi, F.P. Silva, L.L.R. Vono, P.K. Kiyohara, E.L. Duarte, R. Itri, R. Landers, G. Machado, Green Chem. 9 (2007) 379–385.
[19] L.M. Rossi, L.L.R. Vono, F.P. Silva, P.K. Kiyohara, E.L. Duarte, J.R. Matos, Appl. Catal. A: Gen. 330 (2007) 139–144.
[20] L.M. Rossi, I.M. Nangoi, N.J.S. Costa, Inorg. Chem. 48 (2009) 4640–4642.
[21] F.W. Zhang, J. Jin, X. Zhong, S.W. Li, J.R. Niu, R. Li, J.T. Ma, Green Chem. 13 (2011) 1238–1243.
[22] D. Guin, B. Baruwati, S.V. Manorama, Org. Lett. 9 (2007) 1419–1421.
[23] A.J. Amali, R.K. Rana, Green Chem. 11 (2009) 1781–1786.
[24] M.J. Jacinto, P.K. Kiyohara, S.H. Masunaga, R.F. Jardim, L.M. Rossi, Appl. Catal. A: Gen. 338 (2008) 52–57.
[25] V. Mévellec, A. Nowicki, A. Roucoux, C. Dujardin, P. Granger, E. Payen, K. Philippot, New J. Chem. 30 (2006) 1214–1219.
[26] L. Barthe, A. Denicourt-Nowicki, A. Roucoux, K. Philippot, B. Chaudret, M. Hemati, Catal. Commun. 10 (2009) 1235–1239.
[27] C. Hubert, E. Guyonnet Bile, A. Denicourt-Nowicki, A. Roucoux, Green Chem. 13 (2011) 1766–1771.
[28] C. Hubert, A. Denicourt-Nowicki, P. Beaunier, A. Roucoux, Green Chem. 12 (2010) 1167–1170.
[29] E. Guyonnet Bile, R. Sassine, A. Denicourt-Nowicki, F. Launay, A. Roucoux, Dalton Trans. 40 (2011) 6524–6531.
[30] C. Hubert, A. Denicourt-Nowicki, J.P. Guegan, A. Roucoux, Dalton Trans. (2009) 7356–7358.
[31] E. Redel, J. Krämer, R. Thomann, C. Janiak, J. Organomet. Chem. 694 (2009) 1069–1075.
[32] A. Gual, C. Godard, S. Castillon, C. Claver, Dalton Trans. 39 (2010) 11499– 11512.
[33] L. Petrus, M.A. Noordermeer, Green Chem. 8 (2006) 861–867.